J. Fluid Mech. (1994), *vol.* 277, *pp.* 55–83

Nonlinear long-wave stability of superposed fluids in an inclined channel

By B. S. TILLEY[1], S. H. DAVIS[1] AND S. G. BANKOFF[2]

[1] Department of Engineering Sciences and Applied Mathematics, Northwestern University, Evanston, IL 60208, USA

[2] Department of Chemical Engineering, Northwestern University, Evanston, IL 60208, USA

(Received 4 January 1994 and in revised form 2 May 1994)

We consider the two-layer flow of immiscible, viscous, incompressible fluids in an inclined channel. We use long-wave theory to obtain a strongly nonlinear evolution equation which describes the motion of the interface. This equation includes the physical effects of viscosity stratification, density stratification, and shear. A weakly nonlinear analysis of this equation yields a Kuramoto–Sivashinsky equation, which possesses a quadratic nonlinearity. However, certain physical situations exist in two-layer flow for which modifications of the Kuramoto–Sivashinsky equation are physically pertinent. In particular, the presence of the second layer can mediate the wave-steepening instability found in single-phase falling films, requiring the inclusion of a cubic nonlinearity in the weakly nonlinear analysis. The introduction of the cubic nonlinearity destroys the symmetry-breaking bifurcations of the Kuramoto–Sivashinsky equation, and new isolated solution branches emerge as the strength of the cubic nonlinearity increases. Bistability between these new solutions and those associated with the Kuramoto–Sivashinsky equation is found, as well as the formation of a hysteresis loop from smaller-amplitude travelling waves to larger-amplitude travelling waves. The physical implications of these dynamics to the phenomenon of laminar flooding in a channel are discussed.

1. Introduction

Consider the flow of two superposed viscous, incompressible fluids in an inclined channel and separated by an interface. The fluids flow under the joint influence of gravity and an imposed pressure gradient. In this system, several possible physical mechanisms can lead to instability of parallel flow. One expects that inertially driven instabilities found in thin liquid films would be present, along with the mechanisms present when the fluids are distinct. Two-phase flow instabilities can be caused by stratification of density or by viscosity stratification through shear.

The mechanism for the instability of thin liquid films has been studied since Yih (1955) and Benjamin (1957) analysed the linear stability for long waves. Benney (1966) derived a long-wave evolution equation describing the nonlinear interface motion. Smith (1990) described how initial perturbations on a thin film are driven by a perturbation shear stress at the interface with growth provided by inertia. Joo, Davis & Bankoff (1991) integrated Benney's equation numerically to find that waves can steepen and increase to a range where the long-wave assumptions cease to be valid. Waves steepen since wave speeds increase with the interfacial height, that is, peaks travel faster than troughs. The net result of this effect is that more fluid is 'pumped' into the peak from the trough, until hydrostatic effects balance the growth. When the

upper phase is no longer passive, the perturbation shear stress caused by the deflection of the interface will change. Chang (1986) used a phenomenological model to allow for the imposition of a turbulent shear stress on the interface by an otherwise passive second phase, and derived a Kuramoto–Sivashinsky (KS) equation, valid for long waves, in a frame moving with the linear phase speed. Chen & Chang (1986) then investigated spatially periodic solutions of this equation and found that as inertial effects are increased there are transitions to chaotic behaviour.

Since then, the dynamical behaviour of spatially periodic solutions to the KS equation has been explored at length (e.g. see Kevrekidis, Nicolaenko & Scovel 1990; Papageorgiou & Smyrlis 1991; Demekhin, Todarev & Shkadov 1991; Scovel, Kevrekidis & Nicolaenko 1988; Aston, Spence & Wu 1992*a*, *b*). The initial dynamics beyond linear theory consists of a primary steady-state branch, which then loses stability in a symmetry-breaking bifurcation to a pair of travelling waves as the bifurcation parameter is increased. These travelling waves are the images of each other, and travel in opposite directions with the same phase speed. However, the bifurcation to travelling waves is a pitchfork, which is known to be structurally unstable to certain small perturbations. Later, we shall focus on small and large perturbations of the KS equation, and their physical consequences.

For the case of two-layer flow in a horizontal channel, the initiating mechanism for long-wave instability is different. The viscosity–stratification instability found by Yih (1967) is manifested through differences in the tangential-velocity gradient across the interface. Density stratification acts to modify stability, via a Rayleigh–Taylor mechanism. Independently, Schlang (1984) and Hooper & Grimshaw (1985) derived KS equations to describe small-amplitude motion of the interface in a horizontal channel. Further, Schlang (1984) derived a similar equation for two cocurrent fluids in a vertical channel, but did not consider countercurrent flow, or certain other cases which we consider in this work. In a study of the thin-annular limit of vertical core-annular flow, Papageorgiou, Maldarelli & Rumschitzki (1990) derived a KS equation, containing an additional integral term representing the effect of the core flow on the interfacial motion; the motions in the core are not necessarily long waves. Numerical integration of this equation revealed large-amplitude travelling waves in regions of parameter space where the KS equation has chaotic solutions.

A phenomenon called flooding is found in countercurrent flow. It is characterized as the transition from countercurrent flow to cocurrent flow adverse to gravity as the adverse pressure gradient is increased. During this transition, a variety of interfacial dynamics is observed, ranging from possibly chaotic small-amplitude waves to large-amplitude waves that impede the flow of the second phase. Countercurrent flow returns only after the pressure gradient is decreased below the flooding point, a process which is called flow reversal. Bankoff & Lee (1986) reviewed the wide variety of theoretical and experimental attempts to explain the phenomenon, and argued that the analyses are inconclusive. Fowler & Lisseter (1992) have used a phenomenological model to examine flooding in core-annular flow, and found a hysteresis loop between countercurrent and cocurrent states.

Our motivation in the present work is to find a fundamentally based criterion for laminar flooding. In this quest, we fix the total volumetric-flow rate and derive a strongly nonlinear interfacial equation valid in a long-wave regime. A small-amplitude analysis of similar equations for single-phase thin films local to a laminar solution yields a Kuramoto–Sivashinsky equation. However, in the two-fluid problem, certain physical situations require a different scaling that leads to an additional cubic nonlinearity to the KS equation. We compare the bifurcation diagrams for spatially

periodic solutions of these two equations. In particular, we find that the cubic nonlinearity can lead to a hysteresis loop between smaller-amplitude waves and larger-amplitude waves. Such a transition is known to occur near the onset of flooding. We compare the limit in which both nonlinearities are physically important to a phenomenologically based turbulent model, which is used in predicting the onset of flooding. Qualitative agreement is seen between the two models.

This paper is organized as follows. In §2, we derive a strongly nonlinear evolution equation describing the motion of the interface for long waves. Then, we perform a weakly nonlinear analysis on this equation to derive a Kuramoto–Sivashinsky equation in §3. Further, we discuss how certain physical situations allow for the inclusion of both quadratic and cubic nonlinearities in the weakly nonlinear analysis. In §4, we perform a bifurcation analysis for the spatially periodic solutions of both small-amplitude equations as the magnitude of the cubic nonlinearity is increased. In §5, we compare the limit where the cubic nonlinearity is pertinent to a phenomenological model used in the prediction of turbulent flooding. We close with a discussion of the physical implications of these results to the phenomenon of flooding in §6.

2. Derivation of the evolution equation

Two immiscible, incompressible fluids, labelled $i = 1, 2$, fill an inclined channel of depth d, as shown in figure 1. The equations that govern this system are continuity and Navier–Stokes:

$$\nabla \cdot \boldsymbol{u}^{(i)} = 0, \tag{2.1a}$$

$$\rho_i\left(\frac{\partial \boldsymbol{u}^{(i)}}{\partial t} + \boldsymbol{u}^{(i)} \cdot \nabla \boldsymbol{u}^{(i)}\right) = -\nabla p^{(i)} + \rho_i \boldsymbol{g} + \mu_i \nabla^2 \boldsymbol{u}^{(i)}, \tag{2.1b}$$

where $\boldsymbol{u}^{(i)}$, and $p^{(i)}$ are the velocities and pressures of the fluid in each phase, and μ_i and ρ_i are the corresponding dynamic viscosities and densities. The velocities satisfy the no-slip boundary conditions on the channel walls: $\boldsymbol{u}^{(1)} = 0$ on $z = 0$ and $\boldsymbol{u}^{(2)} = 0$ on $z = d$, as well as the following interface conditions at $z = h(x, t)$:

$$[\boldsymbol{n} \cdot \boldsymbol{T} \cdot \boldsymbol{n}] = \sigma\kappa, \tag{2.2a}$$

$$[\boldsymbol{t} \cdot \boldsymbol{T} \cdot \boldsymbol{n}] = 0, \tag{2.2b}$$

$$[\boldsymbol{u} \cdot \boldsymbol{n}] = 0, \tag{2.2c}$$

$$[\boldsymbol{u} \cdot \boldsymbol{t}] = 0, \tag{2.2d}$$

$$h_t + \frac{\partial}{\partial x}\int_0^h u \, \mathrm{d}z = 0, \tag{2.2e}$$

where $\boldsymbol{n}$ is the unit normal pointing from phase 1 into phase 2, $\boldsymbol{t}$ is the unit tangent vector at the interface, $\boldsymbol{T}^{(i)}$ is the stress, σ is the interfacial tension between the two fluids, and κ is twice the mean curvature of the interface, given by

$$\kappa = -h_{xx}(1 + h_x^2)^{-3/2}.$$

The jump $[f]$ of the quantity f across the interface is denoted by $[f] = f^{(2)} - f^{(1)}$.

The constant flow rate $\hat{Q}$ for the full channel is given by

$$\int_0^d u \, \mathrm{d}z = \hat{Q}.$$

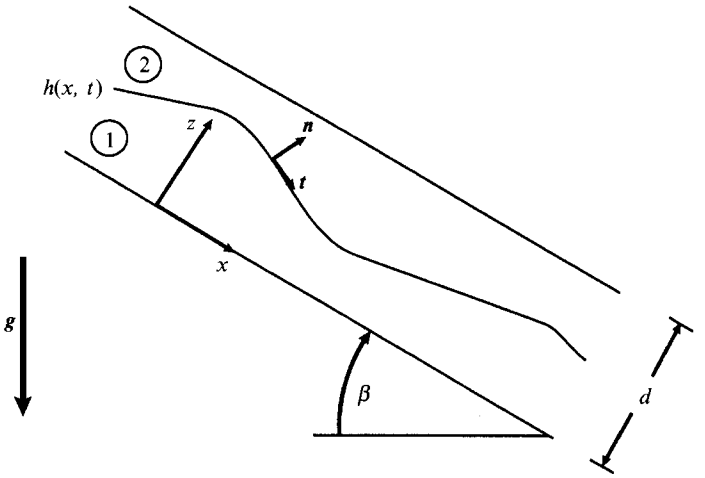

FIGURE 1. Configuration of two-layer flow in an inclined channel.

By integrating the continuity equation across the channel, one can show that

$$\frac{\partial}{\partial x}\int_0^d u\,\mathrm{d}z = [\boldsymbol{u}\cdot\boldsymbol{n}] = 0. \tag{2.3}$$

We scale lengths by d, time by d^2/ν_1, velocities by d/ν_1, and pressures by $\rho_1\nu_1^2/d^2$, where ν_1 is the kinematic viscosity of the lower fluid, to get the dimensionless governing equations:

$$\nabla\cdot\boldsymbol{u}^{(i)} = 0, \tag{2.4a}$$

$$\frac{\partial\boldsymbol{u}^{(i)}}{\partial t}+\boldsymbol{u}^{(i)}\cdot\nabla\boldsymbol{u}^{(i)} = -\frac{\rho_1}{\rho_i}\nabla p^{(i)}+\frac{d^3}{\nu_1^2}\boldsymbol{g}+\frac{\nu_i}{\nu_1}\nabla^2\boldsymbol{u}^{(i)} \quad (i=1,2), \tag{2.4b}$$

with the boundary conditions at the channel walls

$$\boldsymbol{u}^{(1)} = 0 \quad \text{on} \quad z = 0, \tag{2.5a}$$

$$\boldsymbol{u}^{(2)} = 0 \quad \text{on} \quad z = 1, \tag{2.5b}$$

and at the interface $z = h(x,t)$

$$p^{(1)}-p^{(2)}+2\left[\frac{\mu_i/\mu_1}{1+h_x^2}\{(h_x^2-1)u_x-h_x(u_z+w_x)\}\right] = -\bar{\sigma}\frac{h_{xx}}{(1+h_x^2)^{3/2}}, \tag{2.6a}$$

$$\left[\frac{\mu_i}{\mu_1}\{(1-h_x^2)(u_z+w_x)-4h_x u_x\}\right] = 0, \tag{2.6b}$$

$$[u+wh_x] = 0, \quad h_t+\frac{\partial}{\partial x}\int_0^h u\,\mathrm{d}z = 0, \tag{2.6c, d}$$

and with the global constraint

$$\int_0^1 u\,\mathrm{d}z = Q, \tag{2.7}$$

which is equivalent to the interfacial condition of continuity of normal velocity. The following parameters appear:

$$Q = \frac{\hat{Q}}{\nu_1}, \tag{2.8a}$$

$$G = \frac{gd^3}{\nu_1^2}, \tag{2.8b}$$

$$\rho = \frac{\rho_2}{\rho_1}, \tag{2.8c}$$

$$\mu = \frac{\mu_2}{\mu_1}, \tag{2.8d}$$

$$\nu = \frac{\nu_2}{\nu_1}, \tag{2.8e}$$

$$\bar{\sigma} = \frac{\sigma d}{\rho_1 \nu_1^2}. \tag{2.8f}$$

From the full linear stability analysis of this problem, Tilley, Davis & Bankoff (1994) found that, for a broad range of parameters, the primary instability from the flat-interface solution will occur at zero wavenumber as the total volumetric flow rate is increased. Hence, we are concerned with the stability of the interface to long-wave disturbances, and we let $0 < \epsilon \ll 1$ be a measure of the wavenumber. We let $\xi = \epsilon x$, $\zeta = z$, and since we expect all terms in the kinematic boundary condition to be of the same order of magnitude, we introduce a slow timescale $\tau = \epsilon t$. We assume a regular perturbation expansion in u:

$$u^{(i)}(\xi, \zeta, \tau) = u_0^{(i)}(\xi, \zeta, \tau) + \epsilon u_1^{(i)}(\xi, \zeta, \tau) + \epsilon^2 u_2^{(i)}(\xi, \zeta, \tau) + \ldots. \tag{2.9}$$

This assumption and the continuity equation suggest that

$$w^{(i)}(\xi, \zeta, \tau) = \epsilon\{w_0^{(i)}(\xi, \zeta, \tau) + \epsilon w_1^{(i)}(\xi, \zeta, \tau) + \epsilon^2 w_2^{(i)}(\xi, \zeta, \tau) + \ldots\}. \tag{2.10}$$

Finally, we expect downstream pressure gradients to be of unit order. Thus

$$p^{(i)}(\xi, \zeta, \tau) = \epsilon^{-1}\{P_0^{(i)}(\xi, \zeta, \tau) + \epsilon P_1^{(i)}(\xi, \zeta, \tau) + \epsilon^2 P_2^{(i)}(\xi, \zeta, \tau) + \ldots\}. \tag{2.11}$$

We assume large surface tension, and define the unit-order parameter $\bar{S}$:

$$\bar{S} = \epsilon^2 \bar{\sigma}. \tag{2.12}$$

These assumptions induce the following boundary conditions:

$$u_j^{(1)} = w_j^{(1)} = 0 \quad \text{on} \quad \zeta = 0, \tag{2.13a}$$

$$u_j^{(2)} = w_j^{(2)} = 0 \quad \text{on} \quad \zeta = 1, \tag{2.13b}$$

for $j = 0, 1, 2, \ldots$.

At the interface $\zeta = h(\xi, \tau)$, the jump in the tangential component of the velocity becomes

$$[u_0] = 0, \tag{2.14a}$$

$$[u_1] = 0, \tag{2.14b}$$

$$[u_2 + w_0 h_\xi] = 0, \tag{2.14c}$$

$$\vdots$$

Similarly, the jump in the tangential stress at the interface can be written in the form

$$\left[\frac{\mu_i}{\mu_1}u_{0\zeta}\right] = 0, \tag{2.15a}$$

$$\left[\frac{\mu_i}{\mu_1}u_{1\zeta}\right] = 0, \tag{2.15b}$$

$$\left[\frac{\mu_i}{\mu_1}(u_{2\zeta}+w_{0\xi}-u_{0\zeta}h_\xi^2)\right] = 0, \tag{2.15c}$$

$$\vdots$$

The normal-stress condition at the interface can also be written as

$$[p_0] = 0, \tag{2.16a}$$

$$[p_1] = \bar{S}h_{\xi\xi}, \tag{2.16b}$$

$$p_2^{(1)} - p_2^{(2)} + 2\left[\frac{\mu_i}{\mu_1}(-u_{0\xi}-h_\xi u_{0\zeta})\right] = 0, \tag{2.16c}$$

$$\vdots$$

Finally, the integral constraint becomes

$$\int_0^1 u_0\,\mathrm{d}\zeta = Q, \tag{2.17a}$$

$$\int_0^1 u_1\,\mathrm{d}\zeta = 0, \tag{2.17b}$$

$$\vdots$$

With these boundary conditions at each order, we obtain a sequence of linear problems:

$$O(\epsilon^{-1}): \quad (\rho_1/\rho_i)\,P_{0\zeta}^{(i)} = 0, \tag{2.18a}$$

$$P_0^{(1)} = P_0^{(2)} \quad (\zeta = h(\xi,\tau)), \tag{2.18b}$$

$$O(1): \quad (\nu_i/\nu_1)\,u_{0\zeta\zeta}^{(i)} - (\rho_1/\rho_i)\,P_{0\xi}^{(i)} + G\sin(\beta) = 0, \tag{2.19a}$$

$$(\rho_1/\rho_i)\,P_{1\zeta}^{(i)} = -G\cos(\beta) \quad (\zeta = h(\xi,\tau)), \tag{2.19b}$$

$$u_0^{(1)} = 0 \quad (\zeta = 0), \tag{2.19c}$$

$$u_0^{(2)} = 0 \quad (\zeta = 1), \tag{2.19d}$$

$$[(\mu_i/\mu_1)\,u_{0\zeta}] = 0 \quad (\zeta = h(\xi,\tau)), \tag{2.19e}$$

$$[u_0] = 0 \quad (\zeta = h(\xi,\tau)), \tag{2.19f}$$

$$P_1^{(1)} - P_1^{(2)} = -\bar{S}h_{\xi\xi} \quad (\zeta = h(\xi,\tau)), \tag{2.19g}$$

$$\int_0^1 u_0\,\mathrm{d}\zeta = Q. \tag{2.19h}$$

The solution to the $O(\epsilon^{-1})$ equation is that $P_0^{(1)} = P_0^{(2)} = P_0(\xi,\tau)$. The $O(1)$ x-momentum equation (2.19) yields,

$$u_0^{(1)}(\zeta) = \frac{P_{0\xi} - G\sin\beta}{2}(\zeta^2 + a_1), \tag{2.20a}$$

$$u_0^{(2)}(\zeta) = \frac{P_{0\xi} - \rho G\sin\beta}{2\mu}\{(\zeta-1)^2 + a_2(\zeta-1)\}, \tag{2.20b}$$

which satisfy the no-slip boundary conditions (2.13). With the continuity of shear-stress and tangential velocity conditions applied at the interface, we have a second-order linear system to solve for a_1 and a_2. The result of this calculation yields:

$$a_1(h) = a_{11}(h) - \frac{P_{0\xi} - \rho G \sin\beta}{\mu(P_{0\xi} - G\sin\beta)} a_{12}(h),$$

$$a_2(h) = a_{21}(h) + \frac{\mu(P_{0\xi} - G\sin\beta)}{P_{0\xi} - \rho G\sin\beta} a_{22}(h),$$

where

$$a_{11} = \frac{2h(h-1) - \mu h^2}{(\mu-1)h+1},$$

$$a_{12} = \frac{\mu(h-1)^2}{(\mu-1)h+1},$$

$$a_{21} = \frac{(h-1)[(h-1) - 2\mu h]}{(\mu-1)h+1},$$

$$a_{22} = \frac{h^2}{(\mu-1)h+1}.$$

However, we still need to solve for the leading-order pressure gradient. We use the integral constraint (2.7) to find that

$$P_{0\xi} = \frac{2\mu Q + G\{\mu f_1(h,\mu) - \rho f_2(h,\mu)\}\sin\beta}{\mu f_1(h,\mu) - f_2(h,\mu)}, \tag{2.21}$$

where

$$f_1(h,\mu) = h^2\left\{\frac{h}{3} + \frac{1}{2}\left[\frac{(1-\mu)h(h-1)}{(\mu-1)h+1} - 1\right]\right\}, \tag{2.22a}$$

$$f_2(h,\mu) = (h-1)^2\left\{\frac{h-1}{3} + \frac{1}{2}\left[\frac{(1-\mu)h(h-1)}{(\mu-1)h+1} + 1\right]\right\}. \tag{2.22b}$$

Finally, we can write the leading-order expressions for the x-component of the velocity as

$$u_0^{(1)} = \frac{\mu Q}{\mu f_1 - f_2}\left\{\zeta^2 + \left(a_{11} - \frac{a_{12}}{\mu}\right)\zeta\right\} + \frac{G(1-\rho)\sin\beta}{2[\mu f_1 - f_2]}\{f_2\zeta^2 + (f_2 a_{11} - f_1 a_{12})\zeta\} \tag{2.23a}$$

$$u_0^{(2)} = \frac{Q}{\mu f_1 - f_2}\{(\zeta-1)^2 + (a_{21} + a_{22}\mu)(\zeta-1)\}$$

$$+ \frac{G(1-\rho)\sin\beta}{2[\mu f_1 - f_2]}\{f_1(\zeta-1)^2 + (f_1 a_{21} + f_2 a_{22})(\zeta-1)\}. \tag{2.23b}$$

The leading-order z-momentum equation (2.19) yields

$$P_1^{(1)} = \alpha_1 - G\zeta\cos\beta, \tag{2.24a}$$

$$P_1^{(2)} = \alpha_2 - G\rho\zeta\cos\beta, \tag{2.24b}$$

where the α_i are the lubrication pressures generated by the deformed interface. The boundary condition (2.16b) at $\zeta = h(\xi,\tau)$ gives the relation $\alpha_{1\xi} - \alpha_{2\xi} = \Phi_\xi$, where

$\Phi_\xi = \{(1-\rho)hG\cos\beta - \bar{S}h_{\xi\xi}\}_\xi$. At $O(\epsilon)$, the continuity and x-momentum equations yield

$$w_{0\zeta}^{(i)} = -u_{0\xi}^{(i)}, \tag{2.25a}$$

$$\frac{\nu_i}{\nu_1}u_{1\zeta\zeta}^{(i)} - \frac{\rho_1}{\rho_i}P_{1\xi}^{(i)} = u_{0\tau}^{(i)} + u_0^{(i)}u_{0\xi}^{(i)} + w_0^{(i)}u_{0\zeta}^{(i)}, \tag{2.25b}$$

$$\zeta = 0: \quad u_1^{(1)} = 0, \tag{2.25c}$$

$$\zeta = 1: \quad u_1^{(2)} = 0, \tag{2.25d}$$

$$\zeta = h: \quad u_1^{(2)} - u_1^{(1)} = 0, \tag{2.25e}$$

$$\mu u_{1\zeta}^{(2)} - u_{1\zeta}^{(1)} = 0, \tag{2.25f}$$

$$\int_0^1 u_1\,\mathrm{d}\zeta = 0. \tag{2.25g}$$

With a similar analysis as the previous order, we use the interfacial conditions and the integral constraint to arrive at a unique solution to $u_1^{(i)}$ (see Appendix A). Since we are primarily concerned with deriving an evolution equation for the interface, we give only the form of $u_1^{(1)}$:

$$\begin{aligned} u_1^{(1)} = {} & \frac{Q_I(h,Q,\Lambda)h_\xi}{\mu f_1(h,\mu) - f_2(h,\mu)}\{\mu\zeta^2 + (\mu a_{11}(h,\mu) - a_{12}(h,\mu))\zeta\} \\ & + \frac{\Phi_\xi}{2[\mu f_1(h,\mu) - f_2(h,\mu)]}\{f_2(h,\mu)\zeta^2 + [f_2(h,\mu)a_{11}(h,\mu) - f_1(h,\mu)a_{12}(h,\mu)]\zeta\} \\ & + F^{(1)}(\zeta)h_\xi + \frac{\rho[F^{(2)}(h) - (h-1)F_\zeta^{(2)}(h)] - [\mu F^{(1)}(h) - (h-1)F_\zeta^{(1)}(h)]}{(\mu-1)h+1}h_\xi\zeta, \end{aligned}$$

where $F_\zeta^{(i)}$ is the velocity generated by the nonlinear interaction of the basic state with itself in (2.25),

$$\begin{aligned} Q_I(h,Q,\Lambda) = {} & -\left\{\int_0^h F^{(1)}(\zeta)\,\mathrm{d}\zeta + \frac{1}{\nu}\int_h^1 F^{(2)}(\zeta)\,\mathrm{d}\zeta\right\} \\ & + (\rho F_\zeta^{(2)}(h) - F_\zeta^{(1)}(h))\left(\frac{h(h-1)}{2[(\mu-1)h+1]}\right) \\ & - [\rho F^{(2)}(h) - \mu F^{(1)}(h)]\left[\frac{(h-1)^2 - \mu h^2}{2\mu^2[(\mu-1)h+1]}\right] \end{aligned}$$

is an inertial-flow rate, and $\Lambda = (\mu, \rho, G, \beta, \bar{S})$. The elements of this flow rate include a contribution from the perturbation flow rate generated by $F(h)$, and flow rates generated by jumps in the gradients of the shear stress and tangential velocity across the interface. Finally, to derive the evolution equation for the interface $h(\xi,\tau)$, we use the kinematic boundary condition (2.2) to obtain

$$h_\tau + A(h,Q,\Lambda)h_\xi + \epsilon\{[I(h,Q,\Lambda) + \Pi_H(h,\Lambda)]h_\xi + C(h,\Lambda)h_{\xi\xi\xi}\}_\xi = 0, \tag{2.26}$$

where $A(h,Q,\Lambda)$, $I(h,Q,\Lambda)$, $\Pi_H(h,\Lambda)$, and $C(h,\Lambda)$ are discussed in Appendix A. Advection effects at leading-order are represented by $A(h,Q,\Lambda)$, $I(h,Q,\Lambda)$ is the result of inertial effects, $\Pi_H(h,\Lambda)$ represents hydrostatic-pressure effects, and $C(h,\Lambda)$ corresponds to capillary effects. This equation is a generalized version of the Benney (1966) equation for single-phase falling films. For falling films, inertia provides the initial mechanism for linear instability, with advection contributing to wave steepening

of the growing and propagating disturbance. These mechanisms are also present in the two-layer case with the possibility that the presence of the second phase may enhance or retard the growth of the disturbance. It is interesting to note that these mechanisms act on different timescales, with advection effects occurring on a faster timescale than the remaining mechanisms. However, the quasi-linear leading-order equation reveals that the timescale of advection is dependent on the initial conditions of the interface. We shall see in the next section one example of this behaviour.

Equation (2.26) contains various special cases. One recovers the single-phase falling film result (see Joo *et al.* 1991) when $P_{0\xi} = \mu = \rho = 0$. Further, a linear analysis of the equation about $h = \frac{1}{2}$, with $\rho = 1$ for a horizontal channel, $\beta = 0$, gives the result of Yih (1967) for instability induced by viscosity stratification. The long-wave linear-theory results of Yiantsios & Higgins (1988) for the horizontal channel, and of the inclined channel described in Tilley (1994) have also been verified. The symmetry checks described in Charru & Fabre (1994) have also been verified in the horizontal case.

We have used a long-wave theory to reduce the Navier–Stokes equations in two phases, coupled by an interface, into a single partial difference equation for the height of the interface. The velocity and pressure fields in each phase can be determined once the solution to (2.26) is known. In order for a solution of this equation to be physically relevant, it must satisfy the assumptions that were needed to derive the equation from the full system. In particular, the solution to (2.26) must have a small slope, or $h_\xi = O(1)$, in order for the solution to be physically pertinent. In the next section, we examine small-amplitude solutions of (2.26), and determine how the behaviour of these solutions change as certain parameters are varied.

3. Weakly nonlinear analysis

For the physical system we are considering, there are several methods by which the two fluids can be forced through the channel. One manner is to fix the Reynolds numbers of both fluids, or equivalently the volumetric-flow rates. These constraints require that the pressure gradient be determined by the solution. A second method is to fix one of the Reynolds numbers, and also fix the overall pressure drop in the streamwise direction. In this case, the volumetric-flow rate of the second fluid is determined by the solutions. In general, there are three degrees of freedom to drive the flow of both phases, two of which must be chosen and the third is determined from the solution. The evolution equation of §2 was derived under the condition that the total volumetric-flow rate is fixed.

Owing to the complexity of the evolution equation described above, we consider a small-amplitude analysis in a neighbourhood slightly beyond the linear neutral-stability boundary. It is convenient from the above derivation to let h_0 and Q determine the flow rate of each phase. A Kuramoto–Sivashinsky (KS) equation can be derived in the same manner as Hooper & Grimshaw (1985) did in the case for a horizontal channel local to the laminar state $h(\xi, \tau) = h_0$. From their analysis, our equation takes the form

$$H_T + \frac{\partial A}{\partial h_0}(h_0, Q, \Lambda)\, HH_y + B(h_0, Q, \Lambda)\, H_{yy} + C(h_0, \Lambda)\, H_{yyyy} = 0, \tag{3.1}$$

where

$$h(\xi, \tau) = h_0 + \epsilon H(y, T), \tag{3.2a}$$

$$y = \xi - A(h_0, Q, \Lambda)\tau, \tag{3.2b}$$

$$T = \epsilon\tau. \tag{3.2c}$$

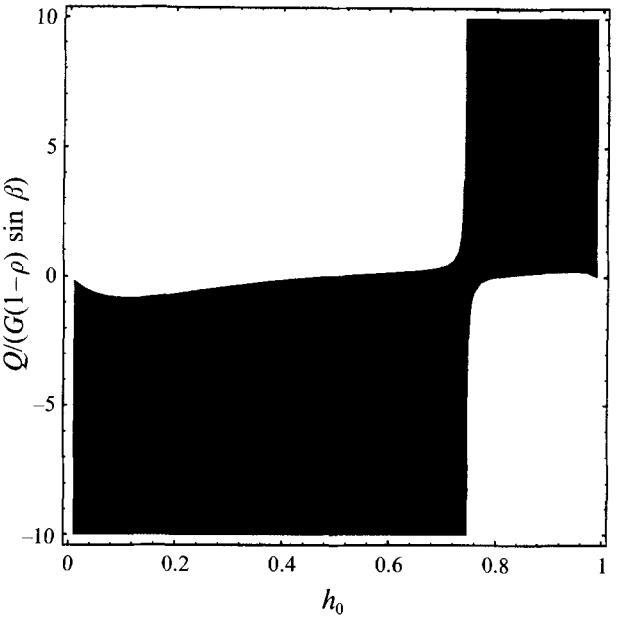

FIGURE 2. Parametric plot of where the wave-steepening coefficient vanishes for an air–water system, where $\partial A/\partial h_0 > 0 (< 0)$ in the unshaded (shaded) region. Notice that the scaling of the total volumetric-flow rate is dependent on the gravitational effects in the direction of the channel walls.

However, there are situations in which

$$\frac{\partial A}{\partial h_0}(h_0, Q, \Lambda) = \frac{6\mu Q}{\Lambda(h_0,\mu)} p_1(h_0,\mu) + \frac{G(1-\rho)\sin\beta}{\Lambda(h_0,\mu)} p_2(h_0,\mu) \tag{3.3}$$

vanishes, where Λ, p_1, and p_2 are shown in Appendix A. We call (3.3) the wave-steepening coefficient. Countercurrent flows fall into the category in which the wave-steepening coefficient is small (see Appendix A), but one also finds that this condition is valid for certain horizontal flows, which are necessarily cocurrent. In figure 2, the shaded regions denote where this wave-steepening coefficient is negative in the mean interfacial height versus scaled total volumetric-flow rate plane for an air–water system. Note that the density ratio, gravity, and the angle of inclination are only present in the scaling of the total volumetric-flow rate, while the zero of the coefficient is a result of the remaining physical quantities. In the context of single-phase thin films, this coefficient is always bounded away from zero. For two-layer flows, when $(\partial A/\partial h_0)(h_0, Q, \Lambda)$ is near zero, cubic terms become important.

Let us consider the possibility that

$$\frac{\partial A}{\partial h_0}(h_0, Q, \Lambda) = \epsilon^{1/2} A_1, \quad A_1 = O(1), \tag{3.4a}$$

$$h(\xi,\tau) = h_0 + \epsilon^{1/2} H(y, T), \tag{3.4b}$$

$$y = \xi - A(h_0, Q, \Lambda)\tau, \tag{3.4c}$$

$$T = \epsilon\tau. \tag{3.4d}$$

If we substitute this ansatz into the evolution equation (2.26), we find that at $O(\epsilon^{3/2})$:

$$H_T + A_1 H H_y + A_2 H^2 H_y + B(h_0, \Lambda) H_{yy} + C(h_0, \Lambda) H_{yyyy} = 0, \tag{3.5}$$

where

$$A_2 = \frac{1}{2}\frac{\partial^2 A}{\partial h_0^2}(h_0, Q, \Lambda).$$

This is a generalization of the KS equation, given the inclusion of the cubic nonlinearity. Balmforth (1993, private communication) has posed a general family of evolution equations, a special case of which is equation (3.5). He has considered this equation in an extended domain, and found a countable set of solitary-wave solutions. However, to the best of the authors' knowledge, this is the first physical situation to be identified in which the cubic nonlinearity is important.

In order to simplify the analysis of this equation, we introduce the new timescale

$$t = C(h_0, \Lambda)\, T, \tag{3.6}$$

and let $x = y, u = H$ to get

$$u_t + u_{xxxx} + \lambda u_{xx} + \alpha u u_x + \gamma u^2 u_x = 0, \tag{3.7}$$

where

$$\lambda = \frac{I(h_0, Q, \Lambda) + \Pi_H(h_0, \Lambda)}{C(h_0, \Lambda)} \tag{3.8}$$

is the ratio of inertial and hydrostatic effects to capillarity, and

$$\alpha = \frac{A_1}{C(h_0, \Lambda)}, \tag{3.9}$$

$$\gamma = \frac{A_2}{C(h_0, \Lambda)}, \tag{3.10}$$

are the ratios to capillarity of the first and second variations of advection with respect to mean interfacial height. For easy reference, we shall call (3.7) the 3KS equation.

The KS equation, which has $\gamma = 0$, possesses translational, reflectional, and Galilean invariances. Translational invariance is present in the full problem, since the streamwise coordinate is an extended domain and the Navier–Stokes equations are based on conservation laws. Hence, it is present in the KS equation. A generalization of reflectional symmetry in the KS equation is seen through the property of replication (see Scovel *et al.* 1988): if $(u(x, t), \lambda, \alpha)$ forms a solution set, then so does $(ku(kx, k^4 t), k^2\lambda, k^2\alpha)$. Reflectional invariance is seen for $k = -1$.

The 3KS equation, which has $\gamma \neq 0$, retains translational invariance, but reflectional and Galilean invariances are absent. A modified replication property exists: if $(u(x, t), \lambda, \alpha, \gamma)$ is a solution, then so is $(ku(kx, k^4 t), k^2\lambda, k^2\alpha, k\gamma)$. Thus, we need only investigate $\gamma \geqslant 0$ to find all solutions with respect to γ. In addition, a nonlinear invariance exists for $\gamma \neq 0$: if $u(x, t)$ is a solution, so is $-\alpha/\gamma - u(x, t)$:

$$u(x, t) \to -\frac{\alpha}{\gamma} - u(x, t). \tag{3.11}$$

To contrast the behaviours of the KS and 3KS equations, we perform a bifurcation analysis on the 3KS equation for spatially periodic solutions as the magnitude of the cubic nonlinearity γ is increased.

4. Bifurcation analysis for spatially periodic solutions

The KS equation has been the subject of extensive study. Kevrekidis *et al.* (1990) considered the KS equation with periodic boundary conditions, and found steady-state bifurcations from the basic state $u = 0$, secondary bifurcations to travelling-wave

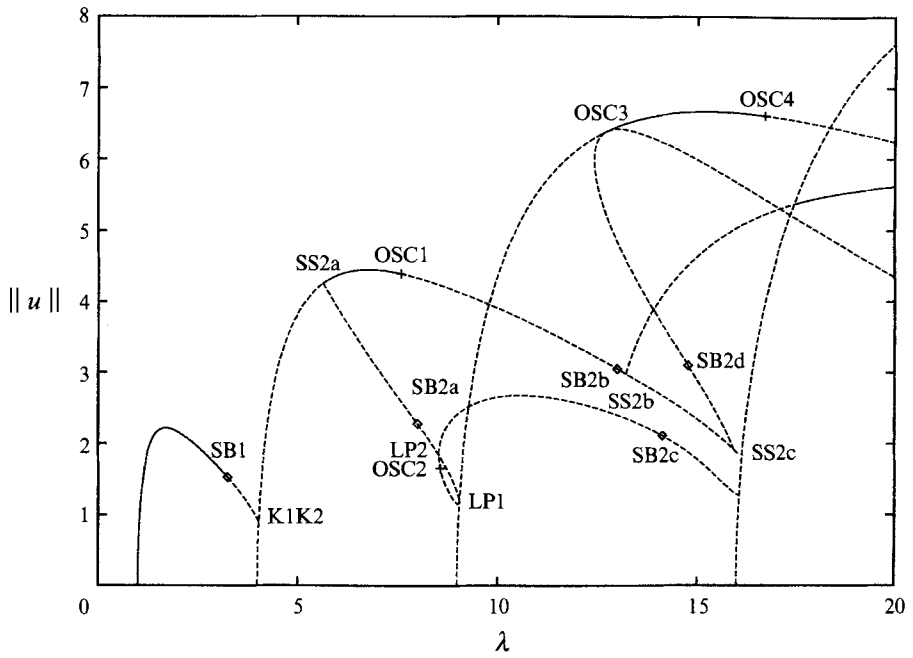

FIGURE 3. Bifurcation diagram for steady-state, spatially periodic solutions of the Kuramoto–Sivashinsky equation: ——, stable solution branches; – – –, unstable solution branches; ◇, bifurcations to travelling-wave solutions, shown in the next figure; +, bifurcations to oscillatory solutions. The labels correspond to the calculated bifurcation-point values listed in table 1.

solutions, and tertiary bifurcations to modulated travelling-wave solutions. As the bifurcation parameter λ is increased further, period-doubling occurs, leading to an intricate web of possible dynamical behaviour (see Demekhin *et al.* 1991; Aston *et al.* 1992*a*, *b*).

We are interested in finding the effect that the cubic nonlinearity has on the bifurcation diagram of the KS equation with periodic boundary conditions. With this in mind, and to compare with previous works of the KS equation, we set $\gamma = 0$, and let $\alpha = \lambda$, since the KS equation can be rescaled to depend only on a single parameter. We review this diagram as a point of reference. Since we are interested in periodic solutions with a fixed total volumetric-flow rate, we consider only zero-mean solutions to the KS equation and the 3KS equation.

Bifurcation points occur on the basic state $u = 0$ for $\lambda = n^2$, $n = 1, 2, \ldots$. An analysis local to these bifurcation points yields a solution of the form

$$u \sim A_n(T) \sin nx$$

at each point, where $A_n(T)$ solves a Landau equation (see Appendix B). This is one of a family of solutions, since any spatial phase shift in the solution is also a solution due to translational invariance.

Figure 3 shows the bifurcation diagram for steady solutions. Stable steady states are shown as solid curves, while the dashed curves denote unstable steady states. Bifurcations to travelling-wave solutions, whose branches are shown in figure 4 for clarity, are marked by diamonds for both figures. The crosses in both figures denote bifurcations to time-periodic solutions (either oscillatory states or modulated travelling-waves), while the square represents a period-doubling bifurcation. The labels of the

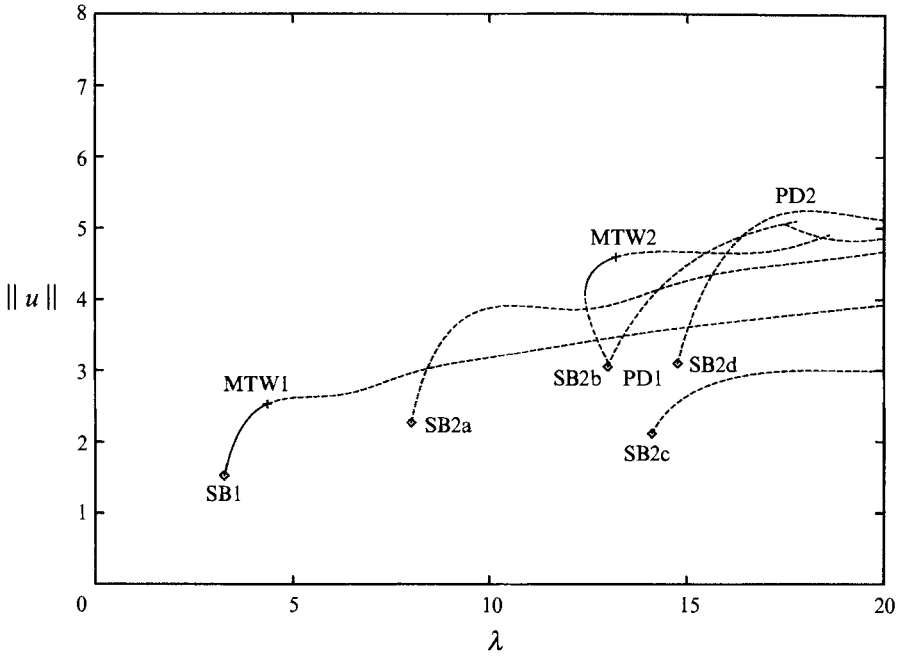

FIGURE 4. Spatially periodic, travelling-wave-solution branches of the Kuramoto–Sivashinsky equation: ——, stable solution branches; – – –, unstable solution branches; +, bifurcations to modulated-travelling-wave solutions; ◇, location of a period-doubling bifurcation. Labels correspond to table 1.

Bifurcation point	TDB λ	KNS (1990) $\lambda = \frac{1}{4}\alpha$	ASW (1992*a*, *b*) $\lambda = \frac{1}{4}\alpha$	DTS (1991) $\lambda = \alpha^{-2}$
SB1	3.250965	3.25125	3.25096	3.2500
K1K2	4.03496	4.034975	—	4.03624
MTW1	4.34934	4.34975	4.349475	4.3493
MTW2	13.2121	—	—	13.2135
OSC1	7.58633	7.5875	—	7.568
OSC2	8.574765	8.575	—	—
OSC3	12.7476	12.724	—	12.73
OSC4	16.7074	—	—	16.673
SS2a	5.639075	5.63975	—	5.63802
SS2b	13.22272	13.2225	—	13.127
SS2c	15.9342	15.934	—	—
SB2a	8.00968	8.0125	8.00966	7.9349
SB2b	13.0038	13.005	—	13.00469
SB2c	14.12395	—	14.12386	14.02
SB2d	14.76810	—	—	14.6798
LP1	9.05854	9.05875	—	—
LP2	8.542285	8.5423	—	—
PD1	13.03555	—	13.03555	13.03298
PD2	17.48108	—	17.48108	—

TABLE 1. Comparison of bifurcation points of the Kuramoto–Sivashinsky equation with previous results. Bifurcation-point labels refer to figures 3 and 4. TDB: our results; KNS, Kevrekidis, Nicolaenko & Scovel; ASW: Aston, Spence & Wu; DTS: Demekhin, Todarev & Shkadov

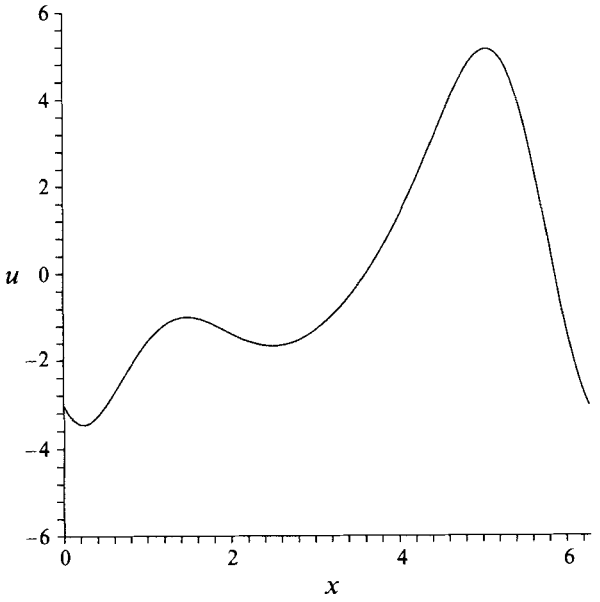

FIGURE 5. KS right-travelling-wave solution for $\lambda = 4.349337$.

bifurcation points refer to table 1, in which we compare our numerical results to those of previous studies.

We note that the basic state $u = 0$ loses stability for $\lambda > 1$. From the pitchfork bifurcation at $\lambda = 1$, a steady-state branch $n = 1$ emerges. Following this branch, a symmetry-breaking bifurcation occurs (see label SB1 in figure 3), from which a branch representing a pair of asymmetric travelling waves emerges, as shown in figure 4. These waves propagate with the same speed, but in opposite directions, and each is locally stable. The spatial structure of this travelling wave is shown in figure 5. The primary steady branch loses stability after this bifurcation, and coalesces with the primary steady-state branch $n = 2$ near $\lambda = 4$ (see K1K2 in figure 3).

The travelling-wave branch in figure 4 undergoes a subcritical bifurcation (not shown) to unstable modulated travelling waves (see MTW1). The travelling-wave branch loses stability after this bifurcation. The modulated travelling-wave solution, as described in Aston *et al.* (1992*b*), represents an oscillation between two spatial structures, and terminates in a heteroclinic orbit.

Following the unstable steady bifurcation solution $n = 2$ from the basic state at $\lambda = 4$, and after the termination of the $n = 1$ steady-state branch, there is an unstable steady bifurcating solution, denoting in figure 3 as SS2a. The $n = 2$ branch then becomes stable, until a bifurcation to oscillatory solutions occurs (see OSC1 in figure 3). The further structure of this branch will not be considered in detail, but is shown for comparison with previous works.

The steady branch which bifurcates from the branch $n = 2$ undergoes bifurcation to travelling waves at $\lambda = 8.009$ and $\lambda = 14.1239$, labelled SB2a and SB2c in figure 3, between which two limit points are seen. It should be noted that the tangent bifurcation was not detected by the method described below, although the full branch was obtained by other means. We show the steady and travelling wave bifurcation diagrams simultaneously in figure 6. Table 1 shows a comparison of our results, TDB, with those of previous works.

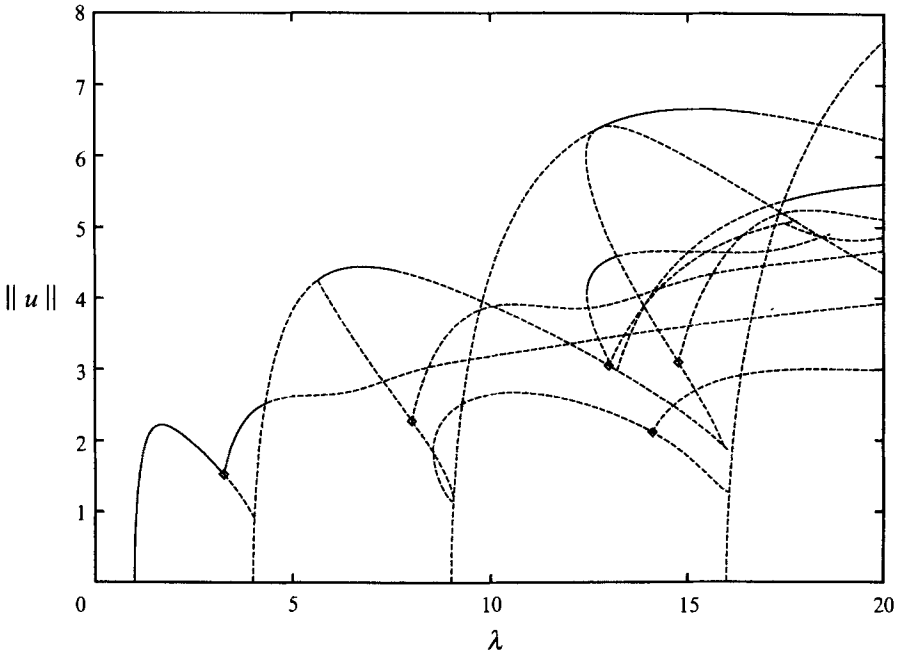

FIGURE 6. Bifurcation diagram of the KS equation with steady-state and travelling-wave branches displayed: ——, stable solution branches; – – –, unstable solution branches; ◇, symmetry-breaking bifurcations.

To determine the bifurcation diagram for the KS equation, as well as the 3KS equation, we use a Galerkin approximation

$$\left.\begin{aligned} u(x,t) &\approx \sum_{k=-N}^{N} a_k(t)\,\mathrm{e}^{\mathrm{i}kx} \\ a_k(t) &= \frac{1}{2\pi}\int_0^{2\pi} u(x,t)\,\mathrm{e}^{-\mathrm{i}kx}\,\mathrm{d}x, \end{aligned}\right\} \tag{4.1}$$

to arrive at a system of ordinary differential equations,

$$\dot{a}_k(t) + (k^4 - \lambda k^2)\,a_k + \tfrac{1}{2}\mathrm{i}\,\lambda k \sum_{j=-N}^{N} a_j\,a_{k-j} + \tfrac{1}{2}\mathrm{i}\gamma \sum_{l=-N}^{N} (k-l)\,a_l \sum_{j=-N}^{N} a_j\,a_{k-j-l} = 0 \quad (k = 1,2,\ldots,N). \tag{4.2}$$

We solve this system using a phase condition described in Aston, Spence & Wu (1991), especially developed for algebraic systems with reflectional and translational symmetries. Two appropriate examples of this phase condition are as follows:

$$\sum_{j=-N}^{N} j a_j^2 = 0, \tag{4.3a}$$

$$\sum_{j=-N}^{N} a_j^2 = 0. \tag{4.3b}$$

In essence, these conditions alter only the eigenvalue corresponding to translational

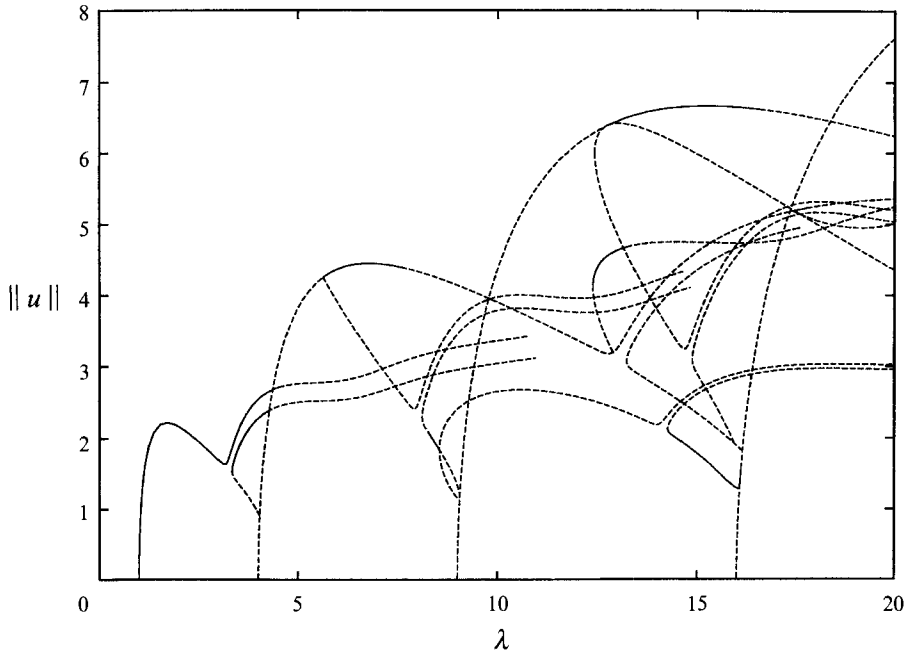

FIGURE 7. Bifurcation diagram for the 3KS equation with $\gamma = 0.1$: ——, stable solution branches; – – –, unstable solution branches. Notice that all the solutions are travelling-waves, and that the symmetry-breaking bifurcations shown for the KS equation are destroyed. The upper branch of the imperfection corresponds to the left-travelling wave.

invariance, while leaving the remaining eigenvalues unaffected. By choosing such a phase condition, we can solve (4.2) using standard continuation packages. The bifurcation package AUTO (Doedel 1981) is used to determine the bifurcation diagrams. Starting points for this package were obtained by a perturbation analysis local to the bifurcation points on the basic state. Further, results were compared to an integration of the full 3KS equation, using a pseudo-spectral method in space, and Gear's method in time, with integration errors on the order of 10^{-8} (see Hyman & Nicolaenko 1986). In the numerical results shown below, we use twenty-four spatial modes, i.e. $N = 24$.

When the cubic nonlinearity is included in the KS equation, the local analysis of bifurcations from the basic state shows that the real eigenvalue in the case $\gamma = 0$ becomes complex, resulting in a travelling-wave bifurcating solution of the same form as the steady solution, but with non-zero wavespeed c,

$$c \sim \gamma |u|^2.$$

This effect is seen throughout the bifurcation diagram. In figure 6, we show the full bifurcation diagram of the KS equation with both steady-state solutions and travelling-wave solutions. Stable solutions are shown as solid curves, and dashed curves denote unstable solutions. Diamonds show bifurcation points to travelling-wave solutions. Figure 7 shows a similar portion of the bifurcation diagram of the 3KS equation for $\gamma = 0.1$. The primary branch bifurcation at $\lambda = 1$ is initially a right-travelling wave. However, as the bifurcation parameter gradually approaches the travelling-wave bifurcation point, the wavespeed becomes negative, revealing that the primary branch is a perturbation of the left-propagating travelling wave of the KS

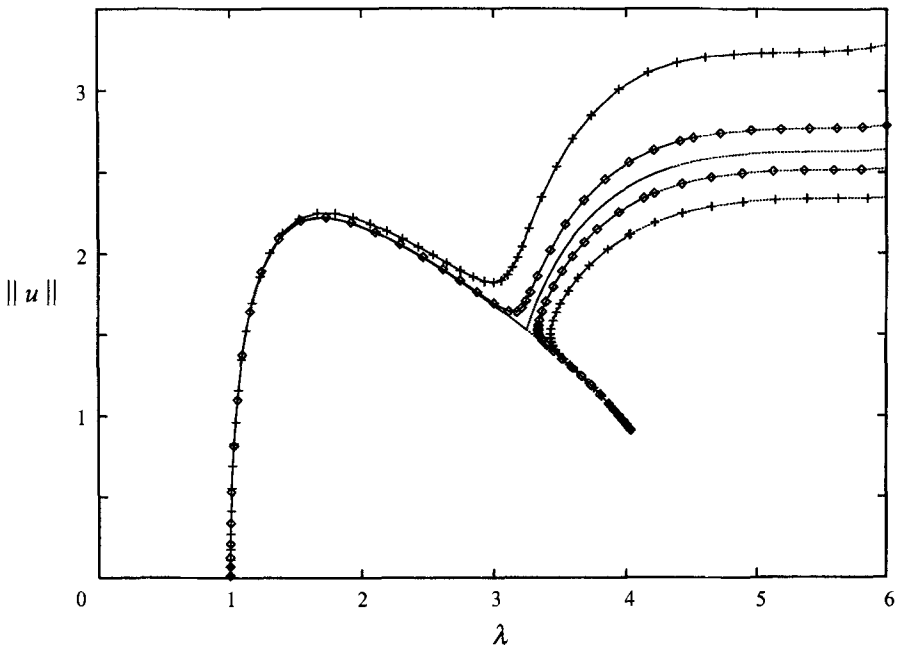

FIGURE 8. Bifurcation diagram of the primary solution branch for 3KS equation for increasing values of γ. Note the imperfect bifurcation in the neighbourhood of $\lambda = 3.25$: ——, stable solution branches; ···, unstable solution branches. Curves with the diamonds are for $\gamma = 0.1$, while those with the crosses are for $\gamma = 0.3$, and the simple curves are for the KS equation $\gamma = 0$.

equation. The corresponding perturbation of the right-travelling wave is also locally stable. Note that not only is the symmetry-breaking bifurcation on the primary branch destroyed, but that all of the bifurcations denoted by diamonds in figure 6 are lost throughout the diagram. This behaviour is generic to pitchfork bifurcations, such as the symmetry-breaking case here, and it has been seen in several contexts (Matkowsky & Reiss 1977; Golubitsky & Schaeffer 1985; Aston 1991). The travelling waves still lose stability through a bifurcation to time-periodic solutions, as in the case $\gamma = 0$. We also remark that the period-doubling bifurcations are not destroyed in the 3KS equation. Further, figure 8 shows the bifurcation diagram for the primary solution branch of the 3KS equation with $\gamma = 0$, $\gamma = 0.1$ and $\gamma = 0.3$. We notice that the range of values of λ for which the left-travelling wave is stable is increased as γ is increased, as shown in figure 9. For the right-travelling wave, this range is decreased. Hence, we see that the result of the inclusion of the nonlinearity not only affects the symmetry-breaking bifurcations of the KS equation, but also changes the domains of stability of the travelling-wave solutions. We shall notice this effect as the value of γ is further increased. In the remainder of this study, we shall concentrate on the behaviour of the primary branch as the strength of the cubic nonlinearity is increased.

A new solution emerges as the strength of the cubic nonlinearity increases. We find an elliptic point at $(\lambda, \gamma) = (12.37, 0.25249)$ from which an isola is formed. This new solution branch represents 'large'-amplitude travelling waves with the upper branch of the isola being locally stable (see figure 10). The size of the isola is sensitive to changes in γ, since figure 10 shows the branch for $\gamma = 0.255566$, just slightly above its formation at $\gamma = 0.25249$. This solution is present only for sufficiently large values of γ, and it is not a solution to the KS equatioin. With a new stable solution in this

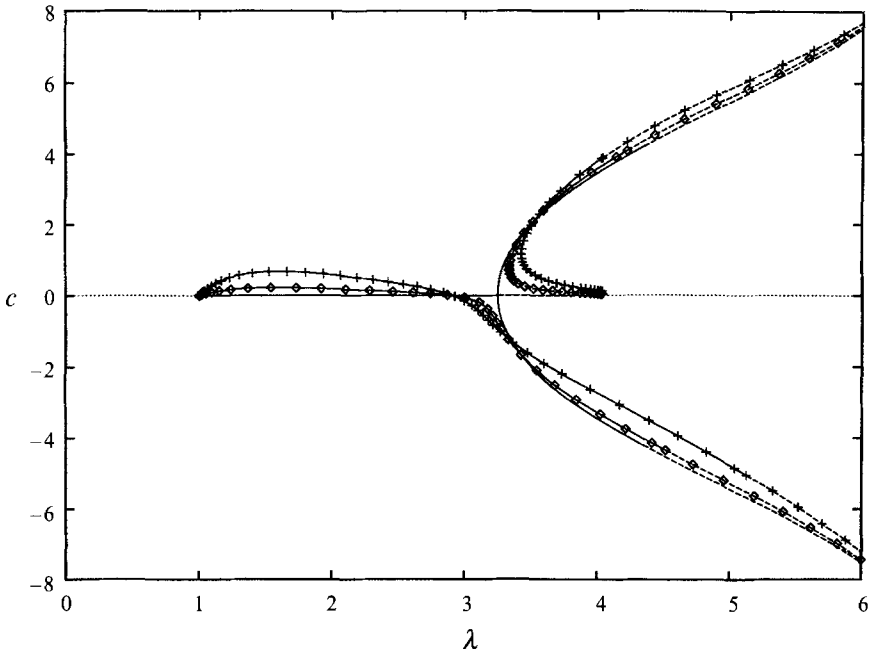

FIGURE 9. Bifurcation diagram of the primary solution branch for the 3KS equation with wavespeed plotted against the bifurcation parameter: ——, stable solution branches; – – –, unstable solution branches. The generic form of the pitchfork imperfection is displayed for small γ. Simple curves denote the wavespeed for the KS solution, while those with diamonds denote the 3KS solutions for $\gamma = 0.1$, and those with the crosses denote 3KS solutions for $\gamma = 0.3$.

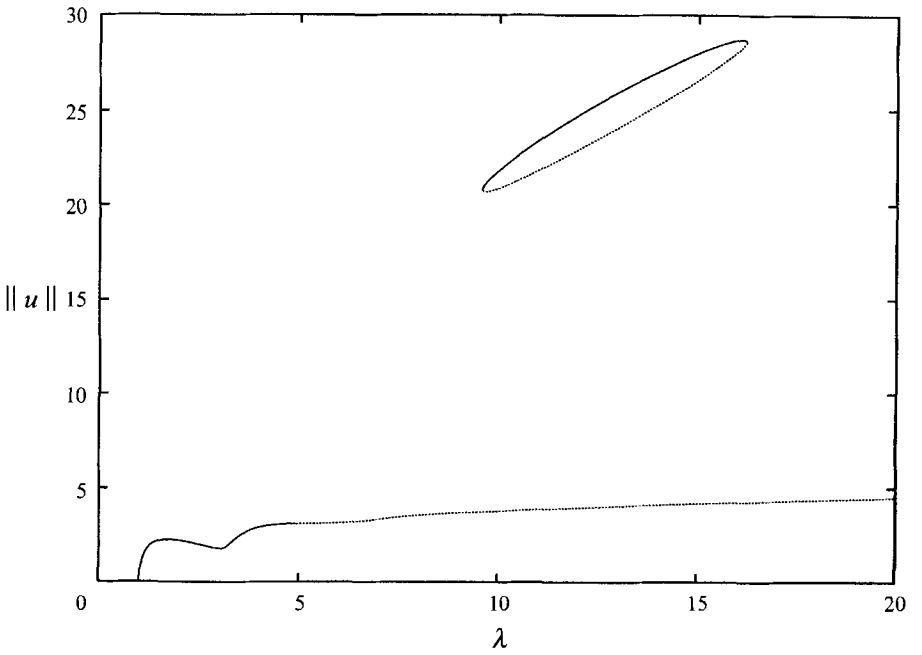

FIGURE 10. The primary and isola solution branches for $\gamma = 0.255566$: ——, stable solutions; ···, unstable solution branches. Notice how sensitive the size of the isola is to variations in γ. $(\lambda, \gamma) = (12.37, 0.25249)$ is the place of elliptic-point formation.

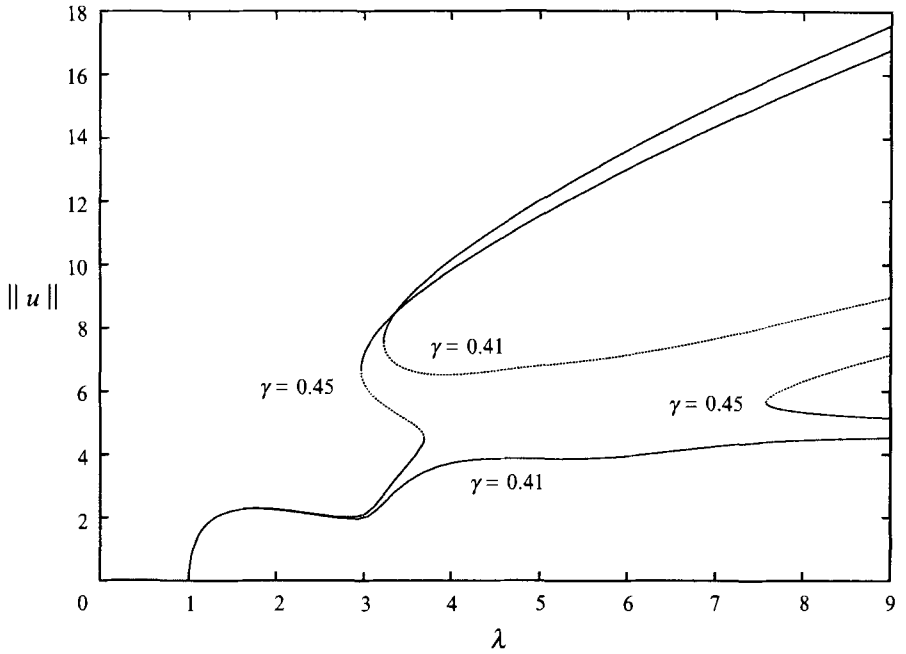

FIGURE 11. Hyperbolic-point bifurcation in the neighbourhood of $\gamma = 0.43$. Notice that the isola solution at $\gamma = 0.41$ merges with the stable primary bifurcating solution: ···, unstable solution branches; ——, stable solution branches.

interval, the domain of attraction for solutions corresponding to solutions of the KS equation are reduced. The implications of this result to multiphase flow will be addressed shortly.

Continuing to increase γ, we find that the isola increases in size, with the unstable portion of the curve approaching the primary bifurcating solution. We show the bifurcation diagram for the isola and the primary bifurcating solution in figure 11 for $\gamma = 0.41$ and $\gamma = 0.45$. Notice for $\gamma = 0.41$ that both the larger-amplitude travelling wave and the primary travelling wave are stable over a wide range of λ. This bistability is of interest physically, since it suggests that significant deflections from a travelling-wave state may lead to attraction to another travelling-wave state. This effect is promoted as γ is increased. When $\gamma = 0.43$, the primary branch and the isola merge through a hyperbolic-point bifurcation, as shown in figure 11. The result of this coalescence is a hysteresis loop along the primary branch. That is, if the bifurcation parameter λ is increased past the location of the limit point at $\lambda = 3.77$, a jump transition from the smaller-amplitude travelling wave to the larger-amplitude travelling wave will occur. Similarly, if the bifurcation parameter is decreased past the limit point at $\lambda = 3.27$ while on the larger-amplitude branch, a jump transition will occur to the smaller-amplitude travelling-wave branch. In figure 12, we show the locally stable travelling-wave solutions of the upper and lower branch with $\lambda = 3.0$ and $\gamma = 0.5$. Notice the differences in amplitude between the two. Further, the speed of the larger wave is $c = 12.80$, while that of the smaller wave is $c = -0.5$.

Further increases to γ result in the branch returning to a supercritical form, with the upper part of the branch displaying a quartic relation between the norm of the solution and λ (see figure 13). This agrees with local asymptotic results of the primary bifurcation when α is small. One expects this, since the small-α equation can be rescaled

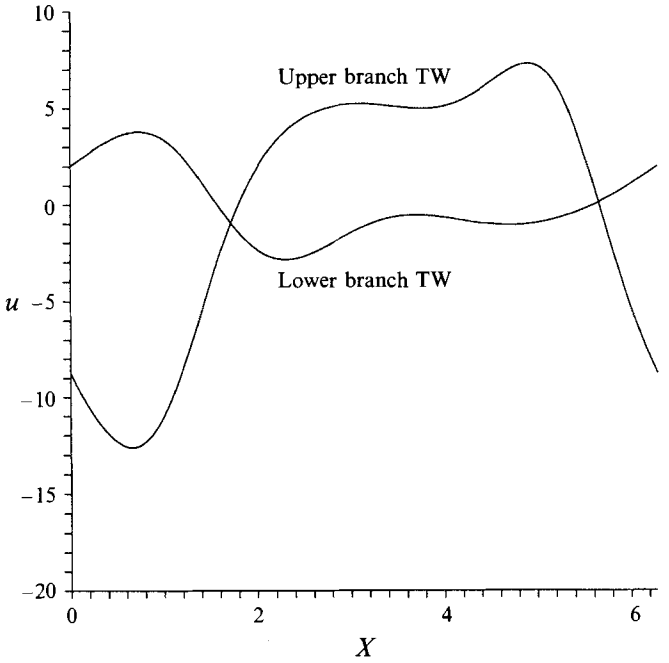

FIGURE 12. Waveform shapes for solutions along the primary branch. Here, $\lambda = 3.0$ and $\gamma = 0.5$. Notice the difference in magnitude.

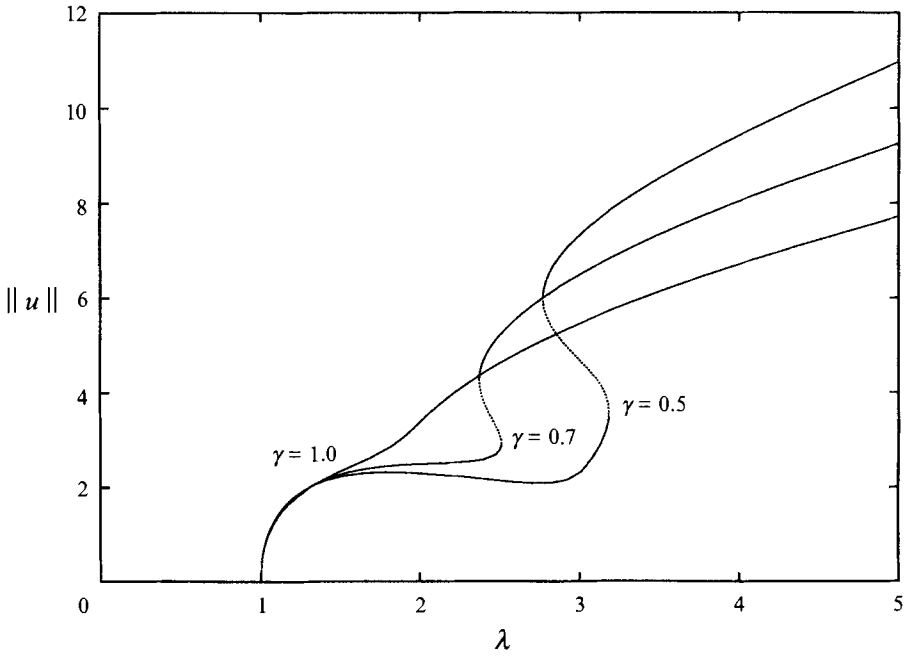

FIGURE 13. Bifurcation diagram for the 3KS equation for increasing values of γ: ——, stable solution branches; ···, unstable solution branches. Notice that the fold singularities are lost, and a quartic relation between the norm and λ is obtained.

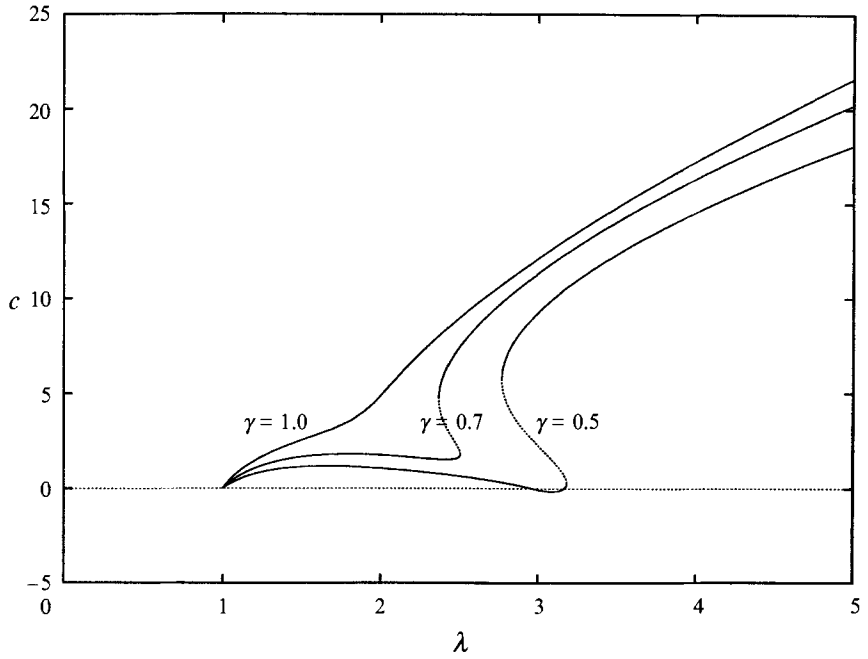

FIGURE 14. Bifurcation diagram for the 3KS equation with wavespeed plotted against the bifurcation parameter for larger γ: ——, stable solution branches; ···, unstable solution branches.

to the 3KS equation with γ large. The effect on phase speed from increasing the strength of the cubic nonlinearity is shown in figure 14.

Through the property of replication, one can understand the stability of spatially periodic solutions of the KS equations to subharmonic disturbances (see Frisch, She & Thual 1986). From their analysis, one finds that there exists a set of wavelengths to which the cellular solutions of the KS equation are unstable. One could perform a similar analysis on the 3KS equation. However, with its modified replication property, there is the possibility of bistability. Even if travelling-wave solutions of the 3KS equation corresponding to the steady-state solutions of the KS equation are unstable to certain subharmonic disturbances, the isolated solutions may be stable to these disturbances. The results of Papageorgiou *et al.* (1990) seem to suggest something of this nature, with the addition of a nonlinear integral term to the KS equation. This equation describes the thin-annular film limit of core-annular flow of two distinct fluids. They report that with the inclusion of the integral term to the KS equation, situations which would yield chaotic solutions for the KS equation instead yield transients which are attracted to travelling-wave states.

5. A comparison of static and dynamic flooding criteria

In this section, we review the separated-cylinders model of Wallis (1969). The model was originally developed to explain the flooding phenomenon in turbulent core-annular flows. In the example of two-layer flow in an inclined channel, one imagines that separate layers of fluid, each of which has a constant average velocity, pass over each other as governed by gravity and an imposed pressure drop. It is assumed that the interface becomes unstable at a critical relative average velocity which is unspecified.

From these assumptions, a relation between the flow rates and the mean interfacial height is derived. We call this criterion a *static-flooding criterion*, since the condition does not include the dynamics of the flow explicitly.

With this in mind, we relate the average velocities with the critical relative velocity v_r

$$\frac{Q_2}{1-h_0}-\frac{Q_1}{h_0}=v_r. \tag{5.1}$$

We introduce the buoyancy sale v_∞

$$v_\infty = G(1-\rho)\sin\beta,$$

and thus define the volumetric-flow rates and velocities

$$q_i = \frac{Q_i}{v_\infty} \quad (i=1,2),$$

$$v_r = r_v v_\infty \quad (r_v < 0),$$

to arrive at

$$\frac{q_2}{1-h_0}-\frac{q_1}{h_0}=r_v. \tag{5.2}$$

To find the maximum flow regimes, and hence a criterion for flooding, we find the envelope of (5.2)

$$\frac{q_2}{(1-h_0)^2}+\frac{q_1}{h_0^2}=0, \tag{5.3}$$

where we have assumed that the flow rates are independent of the mean interfacial height. We note that $q_2 < 0$ and $q_1 > 0$ for countercurrent flows, and thus find the relation for the mean interfacial height in terms of the flow rates

$$h_0 = \frac{|q_1|^{1/2}}{|q_1|^{1/2}+|q_2|^{1/2}}. \tag{5.4}$$

Thus, this static-flooding criterion is given by

$$|q_1|^{1/2}+m|q_2|^{1/2}=|r_v|^{1/2}, \tag{5.5}$$

with, in this case, $m=1$. Empirically, in order to take into acount entrance and exit effects under actual operating conditions, the slope of the straight line is in the range $0.75 < m < 1$. This model still requires the additional value of r_v to determine the flooding criterion, which when found empirically gives $|r_v| \approx 1$.

On the other hand, one can interpret that the presence of the hysteretic behaviour found for the 3KS equation is a precursor to laminar flooding. A necessary criterion for this behaviour to appear is that the wave-steepening coefficient (3.3) is small. Thus, we call the zero of this coefficient a *dynamic-flooding criterion* for laminar flow, which is given by

$$q_D = -\frac{p_2(h_0,\mu)}{p_1(h_0,\mu)},$$

where q_D is the total volumetric-flow rate of both fluids within the channel. In this sense, we have a one-parameter family of criteria, since the mean interfacial height can be imposed based upon the volumetric-flow rate of one of the fluids.

In an experimental situation, the adverse gas flow rate is increased with a fixed liquid

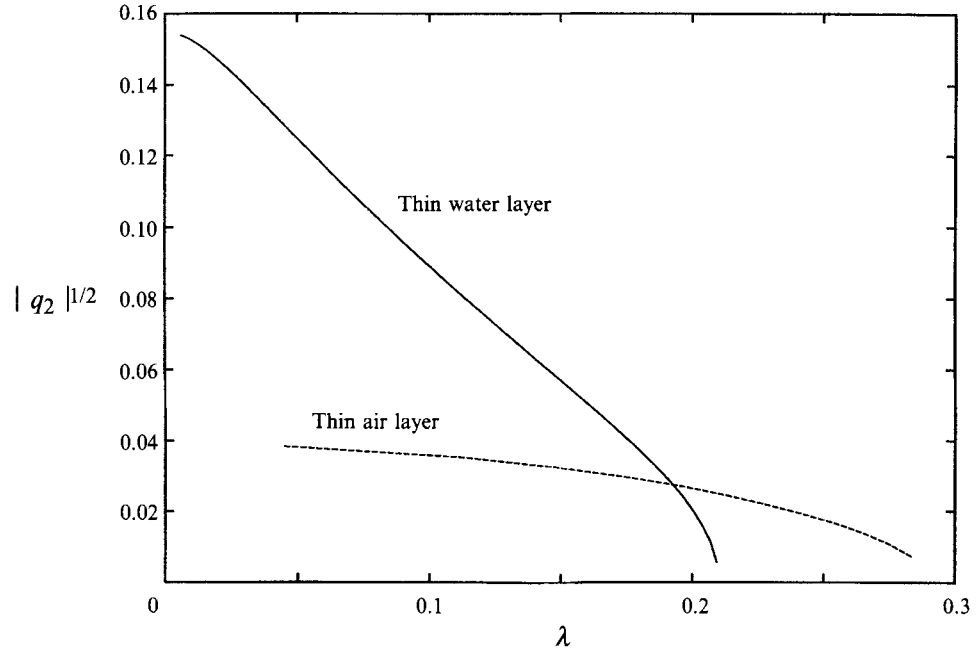

FIGURE 15. Plot of the dynamic-flooding criterion for an air–water system. Notice that the slope of the thin-water-layer branch $m = 0.68$, which is similar to the slope found from the separated-cylinders model of $0.75 < m < 1$.

flow rate until the critical flow rate is achieved. Figure 15, shows the dynamic-flooding criterion for an air–water system, with the upper curve corresponding to countercurrent flow with a thin water layer and the lower curve corresponding to countercurrent flow with a thin air layer. One determines from this figure, given the liquid flow rate q_1, the adverse gas flow rate $|q_2|$ at which the channel 'floods'. The thin-water-layer branch is the one of more practical interest, and we find that the average slope of this branch is $m \approx 0.68$. The fact that the upper curve is nearly a straight line in the $(|q_1|)^{1/2}$ versus $(|q_2|)^{1/2}$ plane is in reasonable agreement to the static-flooding criterion. One would not expect that the critical relative-velocity scale for a turbulent model could be ascertained from a viscous, laminar flow.

The agreement of the slopes of the criteria is a surprising result, since the dynamic-flooding criterion is based on a viscous, laminar flow with strong surface-tension effects, while the separated-cylinders model assumes only a threshold value of the difference in average velocities, in which the wave dynamics of the interface is buried. The agreement may be fortuitous, especially considering the complex nature of actual flooding situations. However, we emphasize that the dynamic-flooding criterion is the first wholly non-empirical model for flooding which has the correct features. We stress that we have found only that there is a correlation between the laminar dynamic-flooding criterion and the turbulent-flow, static-flooding criterion; causation has not been demonstrated. Further, we have assumed that the dynamic-flooding criterion is a necessary condition for flooding and flow reversal to occur. This implies that this condition should be a conservative estimate at best.

6. Conclusions

We have considered the long-wave dynamics of two-layer fluid flow in an inclined channel. In this system, we have assumed that the fluids are immiscible, viscous, and incompressible, and that they possess different physical properties. We have included the effects of gravity, shear, and surface tension. We have studied this system using long-wave theory with our focus centred on the long-wave interfacial stability of two-layer flow. The Reynolds number of each phase is fixed.

Firstly, we derived a strongly nonlinear evolution equation that describes the motion of the interface for long waves. A weakly nonlinear analysis of similar equations in single-phase thin films yields in a moving coordinate frame the Kuramoto–Sivashinsky (KS) equation, where the quadratic nonlinearity is a measure of the wave steepening. However, in two-layer flows, the coefficient of this term can be zero, in which case other nonlinear effects come to the fore. Through a rescaling, one finds in this situation a KS equation with an additional cubic term, which we call the 3KS equation. The inclusion of the cubic nonlinearity breaks the reflectional symmetry found in the KS equation, in addition to the Galilean invariance found in the KS equation.

Next, we compared spatially periodic solutions of the KS equation with solutions of the 3KS equation. Through a weakly nonlinear analysis of the 3KS equation, we found that steady-state solutions of the KS equation become travelling waves in the 3KS equation, with the wave speed proportional to the strength of the cubic nonlinearity and hence the loss of reflectional symmetry. We found that the symmetry-breaking bifurcation of the KS equation from steady-state solutions to travelling-wave solutions is destroyed with the inclusion of the cubic nonlinearity. The structural instability of the symmetry-breaking bifurcation is generic to the unfolding of a pitchfork bifurcation. Further, we noticed that the range of bifurcation parameter values, in which the left-travelling wave is stable, is increased with the inclusion of the cubic nonlinearity, while that of the right-travelling wave is decreased.

As the strength of the cubic nonlinearity is increased, we found the formation of an isolated branch of larger-amplitude travelling waves. These solutions are not related to the KS equation; some of the solutions are locally stable. The size of the isola is sensitive to changes in the strength of the cubic nonlinearity. As the strength of the cubic nonlinearity is further increased, a region of bistability develops. Both the larger-amplitude travelling wave of the isola and the smaller-amplitude left-travelling wave from the KS equation are stable for a given range of total volumetric-flow rates. Further increasing the magnitude of the cubic nonlinearity results in a coalescence of the isola and the primary bifurcating branch, leaving in its wake a hysteresis loop between the smaller- and larger-amplitude travelling waves. Weakening the effect of the quadratic nonlinearity destroys the hysteresis loop, and the quartic relation between the solution amplitude and the bifurcation parameter is approached, as seen in the local analysis of the 3KS equation with no quadratic nonlinearity. We compared the limit in which the 3KS equation describes the weakly nonlinear dynamics to the phenomenologically-based separated-cylinders model, and found qualitative agreement between the two cases.

The physical implications of this analysis are two-fold. First, we are considering the implications of perturbations to the KS equation. As mentioned earlier, the KS equation has been derived in a variety of physical systems, including the description of the interfacial behaviour of single-phase falling film. We have noted that certain perturbations of this equation can change the bifurcation structure, and alter the stability of solutions of the original equation. This behaviour has recently been seen in

a work by Chang, Demekhin & Kopelevich (1993) concerning single-phase falling films. After deriving a system that governs the motion of the interface for moderate Reynolds numbers, they present the bifurcation diagram of the KS equation, and changes which occur when other nonlinear effects are included. These changes include the destruction of the symmetry-breaking bifurcation from cellular solutions to travelling waves. Hence, elements of our study relate as well to the phenomena of single-phase falling films.

The second implication relates to two-phase flows. The 'large'-amplitude solutions found in our study are reminiscent of those seen in Papageorgiou *et al.* (1990). In their study, a core-annular flow is studied in the limit of a thin-annular layer along the cylinder wall. They derive a modified KS equation, with the inclusion of an integral term over the length of the cylinder, which represents the effects of the dynamics of the core on interfacial motion. They report that for parameter ranges where chaotic solutions are found for the KS equation, travelling-wave solutions are seen in their modified equation. This is analogous to the bifurcation diagram of the 3KS equation, where the larger-amplitude travelling waves exist for sufficiently strong cubic nonlinearities. In fact, the cubic nonlinearity in the 3KS equation is a result of the second phase contributing to the dynamics of the interface. Thus, we see that this behaviour is common to both the simpler Cartesian geometry as well as the cylindrical geometry.

Finally, we need to comment on the significance of the hysteresis loop found in this study and the phenomenon of flooding. This hysteresis loop reveals a transition between smaller- and larger-amplitude travelling waves, each transition occurring at a different total volumetric-flow rate. This is reminiscent of the phenomenon of flooding, in the sense that the transition from smaller-amplitude travelling waves to larger-amplitude travelling waves (flooding) occurs at a total volumetric-flow rate beyond the opposite transition (flow reversal). However, we note that the hysteresis loop is derived from a small-amplitude theory, whereas large-amplitude waves, of the order of the channel thickness, are known to appear during the flooding transition. Hence, in order to understand the large-amplitude significance of the hysteresis loop presented here, one must analyse the strongly nonlinear evolution equation derived earlier. From such an analysis, one would be able to better determine the large-amplitude consequences of these jump transitions, and better understand their relation to flooding.

This work was supported by a grant from the Office of Basic Sciences, Department of Energy. BST would also like to thank Professors H. Riecke and A. J. Bernoff for lively discussions and their insights into this problem.

Appendix A. Derivation of the $O(\epsilon)$ portion of the evolution equation with flow rate fixed

We detail the steps in the derivation of the $O(\epsilon)$ correction to the evolution equation for fixed volumetric flow rate.

From (2.25), we can find the first perturbation to the velocity field:

$$\left.\begin{aligned} u_1^{(1)} &= \tfrac{1}{2}\alpha_{1\xi}\zeta^2+\gamma_1\zeta+h_\xi F^{(1)}(\zeta;\Lambda), \\ u_1^{(2)} &= \frac{\alpha_{2\xi}}{2\mu}(\zeta-1)^2+\gamma_2(\zeta-1)+\frac{h_\xi}{\nu}F^{(2)}(\zeta;\Lambda), \end{aligned}\right\} \tag{A 1}$$

where

$$F^{(i)}_{\zeta\zeta} = u^{(i)}_{0r} + u^{(i)}_0 u^{(i)}_{0\xi} + w^{(i)}_0 u^{(i)}_{0\zeta}$$
$$= Q^2 \Gamma^{(i1)}_{\zeta\zeta} + QG(1-\rho)\,\Gamma^{(i2)}_{\zeta\zeta} \sin\beta + [G(1-\rho)\sin\beta]^2\,\Gamma^{(i3)}_{\zeta\zeta},$$

with

$$\Gamma^{(1j)}(\zeta; h, \mu) = g_{1j1}(h;\mu)\,\zeta^6 + g_{1j2}(h;\mu)\,\zeta^5 + g_{1j3}(h;\mu)\,\zeta^4 + g_{1j4}(h;\mu)\,\zeta^3$$
$$\Gamma^{(2j)}(\zeta; h, \mu) = g_{2j1}(h;\mu)(\zeta-1)^6 + g_{2j2}(h;\mu)(\zeta-1)^5$$
$$+ g_{2j3}(h;\mu)(\zeta-1)^4 + g_{2j4}(h;\mu)(\zeta-1)^3.$$

From continuity of tangential velocity, and continuity of shear stress conditions at the interface, we can solve for γ_1 and γ_2 in terms of the pressure gradient perturbations $\alpha_{1\xi}$ and $\alpha_{2\xi}$. Before we proceed, we introduce the convenient notation:

$$[I_v] = \frac{1}{\nu} F^{(2)}(h) - F^{(1)}(h), \tag{A 2}$$

$$[I_{ss}] = \rho F^{(2)}_\zeta(h) - F^{(1)}_\zeta(h), \tag{A 3}$$

where $[I_v]$ is the jump in the x-component of the perturbation velocity due to the inertial interaction of the basic state, and $[I_{ss}]$ is the corresponding jump in perturbation shear stress. Thus, the jump conditions of velocity and shear stress at the interface become:

$$\gamma_1 - \mu\gamma_2 = (h-1)\,\alpha_{2\xi} - h\alpha_{1\xi} + [I_{ss}]\,h_\xi,$$

$$h\gamma_1 - (h-1)\,\gamma_2 = \frac{1}{2\mu}(h-1)^2\,\alpha_{2\xi} - \tfrac{1}{2}h^2\alpha_{1\xi} + [I_v]\,h_\xi,$$

which yields as the solutions

$$\gamma_1 = \frac{a_{11}}{2}\alpha_{1\xi} - \frac{a_{12}}{2\mu}\alpha_{2\xi} + \frac{\mu[I_v] - (h-1)[I_{ss}]}{(\mu-1)h+1} h_\xi,$$

$$\gamma_1 = \frac{\alpha_{11}}{2}\alpha_{1\xi} - \frac{a_{12}}{2\mu}\alpha_{2\xi} + \bar{\gamma}^{(1)} h_\xi,$$

$$\gamma_2 = \frac{a_{22}}{2}\alpha_{1\xi} + \frac{a_{21}}{2\mu}\alpha_{2\xi} + \frac{[I_v] - h[I_{ss}]}{(\mu-1)h+1} h_\xi,$$

$$\gamma_2 = \frac{\alpha_{22}}{2}\alpha_{1\xi} + \frac{a_{21}}{2\mu}\alpha_{2\xi} + \bar{\gamma}^{(2)} h_\xi.$$

To solve for the perturbation pressure gradient terms, we use the solution to the $O(1)$ y-momentum equation at the interface along with the integral constraint to get the system:

$$\alpha_{1\xi} - \alpha_{2\xi} = \Phi_\xi,$$

$$\frac{f_1(h;\mu)}{2}\alpha_{1\xi} - \frac{f_2(h;\mu)}{2\mu}\alpha_{2\xi} = Q_I(h, Q, \Lambda)\,h_\xi.$$

The solution to this system of equations is:

$$\alpha_{1\xi} = \frac{2\mu Q_I(h, Q, \Lambda)\,h_\xi - f_2(h;\mu)\,\Phi_\xi}{\mu f_1(h;\mu) - f_2(h;\mu)},$$

$$\alpha_{2\xi} = \frac{2\mu Q_I(h, Q, \Lambda)\,h_\xi - \mu f_1(h;\mu)\,\Phi_\xi}{\mu f_1(h;\mu) - f_2(h;\mu)},$$

which determines the profile $u_1^{(i)}$ uniquely. We then use the conservation form of the kinematic boundary condition to arrive at the (2.26). The terms are found to be:

$$A(h, Q, \Lambda) = QB_{1h}(h;\mu) + G(1-\rho)\, B_{2h}(h;\mu)\sin\beta, \tag{A 4}$$

$$\begin{aligned} B(h, Q, \Lambda) = {} & G(\rho-1)\cos\beta B_2(h;\mu) \\ & + [I_v]\left\{B_1(h;\mu)\frac{(h-1)^2 - h^2\mu}{2((\mu-1)+1)} + \frac{\mu h^2}{2((\mu-1)+1)}\right\} \\ & + [I_{ss}]\left\{B_1(h;\mu)\frac{h(h-1)}{2((\mu-1)+1)} - \frac{(h-1)h^2}{2((\mu-1)+1)}\right\} \\ & + \{I_Q\}\, B_1(h;\mu) + \int_0^h F^{(1)}(\zeta)\,\mathrm{d}\zeta, \end{aligned} \tag{A 5}$$

$$C(h;\Lambda) = \bar{S}B_2(h;\mu), \tag{A 6}$$

with

$$B_1(h;\mu) = \frac{1}{[\mu f_1 - f_2]}\{\tfrac{1}{3}\mu h^3 + \tfrac{1}{2}h^2(\mu a_{11} - a_{12})\}, \tag{A 7}$$

$$B_2(h;\mu) = \frac{1}{2[\mu f_1 - f_2]}\{\tfrac{1}{3}f_2 h^3 + \tfrac{1}{2}h^2(f_2 a_{11} - f_1 a_{12})\}, \tag{A 8}$$

$$I_Q = \int_0^h F^{(1)}(\zeta)\,\mathrm{d}\zeta + \frac{1}{\nu}\int_h^1 F^{(2)}(\zeta)\mathrm{d}\zeta. \tag{A 9}$$

I_Q is the inertial contribution to the volumetric flow rate of the perturbation velocity field.

The form of $B(h, Q, \Lambda)$ above is given to illustrate the different mechanisms involved. If one simplifies the expression as much as possible with a symbolic manipulator, one finds that it has the form:

$$\begin{aligned} B(h, Q, \Lambda) = {} & G(\rho-1)\, B_2(h;\mu)\cos\beta + Q^2 D_1(h;\mu,\rho) \\ & + QG(1-\rho)\, D_2(h;\mu,\rho)\sin\beta + (G(1-\rho)\sin\beta)^2\, D_3(h;\mu,\rho), \end{aligned} \tag{A 10}$$

with each D_i having the form

$$D_i(h;\mu,\rho) = \rho D_{2i}(h;\mu) - D_{1i}(h;\mu).$$

These terms are ratios of twentieth-degree polynomials in h, with coefficients that are polynomials in μ of, at least, fifth degree. Owing to the complexity of these terms, we refrain from displaying them here, but they are shown in Tilley (1994).

Finally, we show the forms of Δ, p_1, and p_2, as described in the text.

$$\Delta(h_0,\mu) = [(1-h_0)^4 - 2\mu h_0(h_0-1)(h_0^2 - h_0 + 2) + \mu^2 h_0^4]^3,$$

$$\begin{aligned} p_1(h_0,\mu) = {} & 1 - 2h_0 - 12h_0^2 + 56h_0^3 - 98h_0^4 + 84h_0^5 - 28h_0^6 - 8h_0^7 + 9h_0^8 - 2h_0^9 \\ & + \mu h_0^2(12 - 80h_0 + 196h_0^2 - 216h_0^3 + 84h_0^4 + 32h_0^5 - 36h_0^6 + 8h_0^7) \\ & + \mu^2 h_0^3(24 - 114h_0 + 180h_0^2 - 84h_0^3 - 48h_0^4 + 54h_0^5 - 12h_0^6) \\ & + \mu^3 h_0^4(16 - 48h_0 + 28h_0^2 + 32h_0^3 - 36h_0^4 + 8h_0^5) - \mu^4 h_0^7(8 - 9h_0 + 2h_0^2), \end{aligned}$$

$$\begin{aligned} p_2(h_0,\mu) = {} & 2h_0(1-h_0)[(1-h_0)^{11} + \mu h_0(6 - 66h_0 + 295h_0^2 - 734h_0^3 + 1154h_0^4 \\ & - 1226h_0^5 + 916h_0^6 - 490h_0^7 + 184h_0^8 - 44h_0^9 + 5h_0^{10}) + \mu^2 h_0^2(16 - 146h_0 + 508h_0^2 \\ & - 934h_0^3 + 1058h_0^4 - 832h_0^5 + 496h_0^6 - 222h_0^7 + 66h_0^8 - 10h_0^9) + \mu^3 h_0^3(16 - 104h_0 \\ & + 242h_0^2 - 286h_0^3 + 236h_0^4 - 182h_0^5 + 112h_0^6 - 44h_0^7 + 10h_0^8) \\ & - \mu^4 h_0^6(8 - 10h_0 - 11h_0^2 + 19h_0^3 - 11h_0^4 + 5h_0^5 - h_0^6)]. \end{aligned}$$

The characteristic equation is the basis of checking the validity of the evolution equation. Our characteristic equation agrees exactly with that found in Yih (1967), and the numerical calculated examples given in Yiantsios & Higgins (1988). Further, for the inclined case, particular examples were checked with a linear analysis of the full system for arbitrary wavenumber (see Tilley *et al.* 1994).

Appendix B. Weakly nonlinear analysis of the 3KS equation

To find the local behaviour of the 3KS equation local to the bifurcation points $k = 1, 2, \ldots,$ along the basic state, we let

$$\begin{aligned} \lambda &= k^2 + \delta\epsilon^2, \\ \tau &= \epsilon^2 t, \\ u(x,\tau) &= \epsilon u_1(x,\tau) + \epsilon^2 u_2(x,\tau) + \ldots \end{aligned} \tag{B 1}$$

and expand the 3KS equation in powers of ϵ. At $O(\epsilon)$, we find

$$Lu_1 \equiv u_{1xxxx} + k^2 u_{1xx} = 0,$$

which has the solution

$$u_1(x,\tau) = A_1(\tau)\, \mathrm{e}^{\mathrm{i}kx} + \text{c.c.} + B_1(\tau),$$

where c.c. denotes the complex conjugate. At $O(\epsilon^2)$,

$$\begin{aligned} Lu_2 &= -\alpha u_1 u_{1x} \\ &= -\alpha[\mathrm{i}kA_1(\tau)\, B_1(\tau)\, \mathrm{e}^{\mathrm{i}kx} + \mathrm{i}kA_1^2\, \mathrm{e}^{2\mathrm{i}kx} + \text{c.c.}]. \end{aligned}$$

By solvability, $B_1(\tau) = 0$, since $A_1(\tau) = 0$ is simply the basic state. Hence the solution for u_2 is

$$u_2(x,\tau) = A_2(\tau)\, \mathrm{e}^{\mathrm{i}kx} - \frac{\mathrm{i}\alpha}{12k^3} A_1^2\, \mathrm{e}^{2\mathrm{i}kx} + \text{c.c.} + B_2(\tau).$$

At $O(\epsilon^3)$, solvability requires a Landau equation for A_1:

$$\dot{A}_1 = \delta k^2 A_1 - \mathrm{i}k\alpha B_2(\tau)\, A_1(\tau) - \left(\frac{\alpha^2}{12k^2} + \mathrm{i}\gamma k\right) |A_1|^2 A_1. \tag{B 2}$$

At $O(\epsilon^4)$, we find that $\dot{B}_2 = 0$, which shows that the linear effect of a constant perturbation results in a waveform travelling as a function of that wavespeed. This is expected, since the KS equation has the property of Galilean invariance. Since we are concerned with nonlinear effects, we choose $B_2 = 0$.

We can find the solution to (B 2) in the form

$$A_1(\tau) = \rho(\tau)\, \mathrm{e}^{\mathrm{i}\theta(\tau)},$$

to get the system

$$\begin{aligned} \dot{\rho} - k^2\delta\rho + \frac{\alpha^2}{12k^2}\rho^3 &= 0, \\ \rho\dot{\theta} &= -\gamma k\rho^3. \end{aligned}$$

The amplitude equation is Riccati's equation, which has the solution for $\delta > 0$

$$\rho = \pm k^2 \left(\frac{12\delta}{\alpha^2 + 12\delta k^4 \exp(-2k^2\delta\tau)}\right)^{1/2},$$

and for long times approaches a constant value. Thus, we find for long time behaviour

$$|u| \sim (\lambda - k^2)^{1/2},$$
$$c \sim \gamma |u|^2.$$

REFERENCES

ASTON, P. J. 1991 *Physica* D **52**, 415.

ASTON, P. J., SPENCE, A. & WU, W. 1992*a* *SIAM J. Appl. Maths* **52**, 792.

ASTON, P. J., SPENCE, A. & WU, W. 1992*b* *Intl Ser. Numer. Maths* **104**, 35.

BANKOFF, S. G. & LEE, S. C. 1986 In *Multiphase Science and Technology* (ed. G. F. Hewitt, J. M. Delhaye & N. Zuber) p. 95. Hemisphere.

BENJAMIN, T. B. 1957 *J. Fluid Mech.* **2**, 554.

BENNEY, D. J. 1966 *J. Maths Phys.* **45**, 150.

CHANG, H. C. 1986 *Chem. Engng Sci.* **41**, 2463.

CHANG, H. C., DEMEKHIN, E. A. & KOPELEVICH, D. I. 1993 *J. Fluid Mech.* **250**, 433.

CHARRU, F. & FABRE, J. 1994 *Phys. Fluids* **10**, 1223.

CHEN, L. H. & CHANG, H. C. 1986 *Chem. Engng Sci.* **41**, 2477.

DEMEKHIN, Y. A., TODAREV, G. YU. & SHKADOV, V. YA. 1991 *Physica* D **52**, 338.

DOEDEL, E. J. 1981 *Congressus Numerantium* **30**, 265.

DRAZIN, P. G. 1992 *Nonlinear Systems*. Cambridge University Press.

FOWLER, A. C. & LISSETER, P. E. 1992 *SIAM J. Appl. Maths* **52**, 15.

FRISCH, U., SHE, Z. S. & THUAL, O. 1986 *J. Fluid Mech.* **168**, 221.

GOLUBITSKY, M. & SCHAEFFER, D. G. 1985 *Singularities and Groups in Bifurcation Theory*. Springer.

HOOPER, A. P. & GRIMSHAW, R. 1985 *Phys. Fluids* **28**, 37.

HYMAN, J. M. & NICOLAENKO, B. 1986 *Physica* D **18**, 113.

JOO, S. W., DAVIS, S. H. & BANKOFF, S. G. 1991 *J. Fluid Mech.* **230**, 117.

KEVREKIDIS, I. G., NICOLAENKO, B. & SCOVEL, J. C. 1990 *SIAM J. Appl. Maths* **50**, 760.

MATKOWSKY, B. J. & REISS, E. L. 1977 *SIAM J. Appl. Maths* **33**, 230.

PAPAGEORGIOU, D. T., MALDARELLI, C. & RUMSCHITZKI, D. S. 1990 *Phys. Fluids* A **2**, 340.

PAPAGEORGIOU, D. T. & SMYRLIS, Y. S. 1991 *Theoret. Comput. Fluid Dyn.* **3**, 15.

SCHLANG, T. 1984 Nonlinear stability analysis of problems in thin film fluid theory. PhD thesis, Department of Applied Mathematics, Tel Aviv University.

SCOVEL, J. C., KEVREKIDIS, I. G. & NICOLAENKO, B. 1988 *Phys. Lett.* A **130**, 73.

SMITH, M. K. 1990 *J. Fluid Mech.* **217**, 469.

TILLEY, B. S. 1994 Stability of two-layer flow in an inclined channel. PhD thesis, Department of Engineering Sciences and Applied Mathematics, Northwestern University.

TILLEY, B. S., DAVIS, S. H. & BANKOFF, S. G. 1994 Linear stability theory of two-layer fluid flow in an inclined channel. *Phys. Fluids* (to appear).

WALLIS, G. B. 1969 *One-Dimensional Two-Phase Flow*. McGraw-Hill.

YIANTSIOS, S. G. & HIGGINS, B. G. 1988 *Phys. Fluids* **31**, 3225.

YIANTSIOS, S. G. & HIGGINS, B. G. 1989 *Phys. Fluids* A **1**, 1484.

YIH, C. S. 1955 *Proc. 2nd US Congr. Appl. Mech., Am. Soc. Mech. Engrs.* p. 623.

YIH, C. S. 1967 *J. Fluid Mech.* **27**, 337.